chemistry

MDPI

Article

Porous Natural Diamond with Embedded Metal ($Pt_{0.50}$–$Co_{0.50}$)

Evgeny Filatov [1,*], Aleksei Chepurov [2], Valeri Sonin [2], Andrey Zadesenets [1], Sergey Gromilov [1,3] and Egor Zhimulev [2]

[1] Nikolaev Institute of Inorganic Chemistry, Siberian Branch of the Russian Academy of Sciences, Novosibirsk 630090, Russia
[2] Sobolev Institute of Geology and Mineralogy, Siberian Branch of the Russian Academy of Sciences, Novosibirsk 630090, Russia; sonin@igm.nsc.ru (V.S.)
[3] Department of Physics, Novosibirsk State University, Novosibirsk 630090, Russia
* Correspondence: decan@niic.nsc.ru

Abstract: Natural diamond crystals with a highly porous surface were used as substrates for synthesizing single-phase bimetallic Pt–Co nanoparticles at temperatures of 500 °C and 800 °C. The metal nanoparticles inside the pores were determined to take the form of single-phase $Pt_{0.50}Co_{0.50}$ solid solutions with different degrees of superstructure ordering. A detailed characterization of both nanoalloys revealed a tetragonal symmetry with a space group, *P*4/mmm. For the sample obtained at 500 °C, the lattice parameters were a = 2.673(2), c = 3.735(3) Å, and c/a = 1.397(1); for the samples obtained at 800 °C, the parameters were—a = 2.688(2), c = 3.697(3) Å, and c/a = 1.375(1). Within the experimental parameters, no significant chemical interaction of the diamond with the Pt–Co particles was identified. The results demonstrate a strong anchoring effect of the metallic material within the etching pores. The successful synthesis of bimetallic Pt–Co particles embedded inside the caverns can facilitate a study of their magnetic properties. The presence of Pt–Co in specific diamond compositions can also be used for marking diamond crystals as a means for their subtle identification, as well as confirming the possibility of capturing significant amounts of metal along with diamonds during their dissolution in the deep Earth.

Keywords: diamond; Pt–Co; nanoparticles; surface micromorphology; X-ray diffraction; subduction

Citation: Filatov, E.; Chepurov, A.; Sonin, V.; Zadesenets, A.; Gromilov, S.; Zhimulev, E. Porous Natural Diamond with Embedded Metal ($Pt_{0.50}$–$Co_{0.50}$). *Chemistry* **2023**, *5*, 1804–1814. https://doi.org/10.3390/chemistry5030123

Received: 29 June 2023
Revised: 31 July 2023
Accepted: 7 August 2023
Published: 14 August 2023

1. Introduction

The wide field of potential applications of bimetallic alloys continues to expand rapidly. Whether taking the form of bulk materials or nanoscale particles, bimetallic alloys find application in the chemical, electrochemical, and electronics industries. Nano- and ultra-dispersed bimetallic metal particles are actively used for heterogeneous catalysis, which plays a significant role in the chemical and petrochemical industries. Within such processes, platinum group metals are the most commonly used. Thus, the synthesis of bi- and polymetallic nanoparticles is one of the most relevant areas of research in modern chemistry and materials science [1]. Nanoalloys can be produced using a variety of media, such as cluster beams and colloidal solutions, as well as immobilization on surfaces, inside pores, or even in carbon nanotubes [2–5]. Methods of metal reduction from precursor compounds at low temperatures [6,7] play an increasing role due to their relative simplicity, low cost, and the high quality of the final product.

An effective and simple method for producing deposited alloy nanoparticles involves the decomposition of double-complex salts directly inside the pores of a substrate. Double-complex salts (DCSs) of transition metals are compounds containing a complex cation of one metal and a complex anion of another metal. The possibility of implementing an approach based on the decomposition of DCSs directly inside the pores of a support material for catalyst preparation has been demonstrated in a number of works [8–13]. When studying the properties of bimetallic nanoparticles, one of the key factors is the substrate

material on which such particles are deposited, since the choice of substrate material can significantly affect the properties of the final composite [11,12].

The potential use of diamond as a substrate is mainly limited by the fact that most metals slightly wet the diamond surface. Although the contact angle can be significantly decreased by the addition of carbide-forming metals to the alloys [14], progress in this field is in most cases hampered by the weak contact between the diamond and metal and the consequent inability of metal particles to form a strong bond at the diamond surface. At the same time, diamond is a very interesting substrate material due to its many unique properties, including its extreme chemical, mechanical, and radiation resistance, as well as high thermal conductivity and optical transparency [15]. For example, modified diamond electrodes with nanosized metal or metal oxide clusters deposited on their surface are used in various electrochemical applications [16–20]. However, only a few works on the synthesis of bimetallic compounds on diamonds are extant in the literature so far [21–23]. Bimetallic compounds deposited onto boron-doped diamond (BDD) thin-film electrodes comprise a suitable substrate for the electrochemical investigation of supported catalytic nanoparticles. The applicability in electrocatalysis of thermally decomposed electrodeposited Pt particles has been studied; once deposited on the BDD substrate, the particles exhibited electrocatalytic activity [21].

When considering diamond as a substrate material, the nature of the diamond surface should be taken into account. In order to create a certain degree of roughness of the diamond surface, various etching procedures can be used. Among these, the most effective is oxygen [24–26] or hydrogen [27] plasma etching, as well as contact etching using metals in a solid state [28–31]. Such treatments produce etch pits to form a highly porous surface. This raises a number of questions regarding the peculiarities of the synthesis and characterization of metal particles on a porous diamond. Therefore, the present study set out to investigate the synthesis of Pt–Co bimetallic nanoparticles on the porous surface of natural diamond and the characterization of the obtained composite.

2. Materials and Methods

As a substrate material, we used two natural, flat-shaped diamond crystals of octahedral habit. The diamonds were colorless, 2 mm in size, and free of inclusions. The use of natural diamond crystals in this work is due to their ease of etching as compared with other diamond types [29,32]. In order to produce a porous surface on the diamonds, thermochemical etching was carried out using a high-temperature water-cooled microfurnace according to the state assignment of IGM SB RAS. Iron particles were used as an etchant according to the procedure described in our earlier publications [29,32–34]. Following etching, the diamonds were cleaned in acids in order to remove Fe particles, as well as other possible surface contaminants such as graphite, amorphous carbon, or organic compounds. The details of the etched surface of the diamond have been well described in our earlier publication [35].

The synthesis of metal nanoparticles on the etched diamond substrates was carried out with the aim of embedding synthesized nanoparticles of a specific composition in the diamonds. During these experiments, the two CoPt samples deposited on the diamonds were heated to 800 °C and 500 °C. The synthesis of the bimetallic nanoalloys of Pt–Co was carried out with thermolysis of a double-complex salt $[Co(H_2O)_6][Pt(NO_2)_4]\cdot 2H_2O$ containing the required metals (Pt, Co) in an equiatomic ratio. The synthesis procedure and study of the thermal properties of the initial precursor compound have previously been described in detail [36].

A saturated salt solution was applied dropwise to the etched surface of the diamonds. Each subsequent drop was applied following the complete drying of the previous one. This procedure was repeated until the diamond surface turned slightly pink (five drops), corresponding to the color of the initial salt. After the solution dried, the diamond with deposited salt was placed in a quartz reactor of a tubular furnace and heated in a stream of

hydrogen at a rate of 10 K/min. Upon reaching the required temperature, the sample was treated for an hour and then removed from the furnace for rapid cooling (quenching).

The diamond crystal surfaces were examined in CKP "Nanostruktury" (Novosibirsk, Russia) using a scanning electron microscope (LEO 1430 and 1540 XB Crossbeam, Zeiss). The SEM observation was carried out in secondary electron observation mode (emitted from near the specimen surface, within 10 nm of depth) after covering the diamond surface with 10 nm of Al for decharging purposes. Local EDX analysis was carried out using an energy-dispersive X-ray (EDX) spectrometer (EDAX, Pleasanton, CA, USA) fitted with a Si (Li) detector with a resolution of 130 eV. The error in the determination of the metal particle composition was typically not less than 0.5 at %.

X-ray diffraction studies of the obtained samples (diamond single crystal with metal particles deposited on its surface) were carried out using a Bruker APEX DUO diffractometer equipped with a KFF-Mo-2K-90 sharp-focus X-ray tube and the following parameters: graphite monochromatized MoK_α—radiation (λ = 0.70932 Å); collimator—0.35 mm; CCD area detector—4K; resolution—512 × 512; pixel size—0.12 mm; D = 35 mm; $2\theta_D = 42°$. When shooting, reflection geometry was used; the facet of the diamond with the deposited metal layer was turned at an angle in the range of 20–30° relative to the primary beam. The specific angle value was chosen such that diamond reflections did not fall on the detector. During the accumulation of the diffraction pattern (Debye powder pattern), the sample was rotated around the φ axis by 0.5° in 10 min. Si was used as an external reference (SRM-640, a = 5.4309 Å). Amendments and the transition to standard form $I(2\theta)$ were performed using the DIOPTAS program [37]. The X-ray phase analysis was carried out using the PDF database (card numbers: 000-04-0802, 000-15-0806, 000-29-0498, 000-65-8968) [38]. The ICSD database (cards #102621 and #102620) was used for constructing theoretical diffractograms and conducting full-profile refinement [39]. The parameters of the metal phases and degree of superstructural ordering were refined over the entire data array using the Powder Cell 2.4 application [40]. Powder diffraction patterns of metal nanoalloys obtained via thermolysis of the original salt were measured under Cu K_α radiation. For line profile analysis, the instrumental profile was measured using coarse Si powder. Since no increase in accuracy using the fine-structure profile of the Cu K_α doublet was observed, further modeling relied solely on the $K_{\alpha 1/\alpha 2}$ doublet. In order to calculate the order parameter a of the solid solution, the following technique was used. For each of the experimental patterns, the corresponding theoretical pattern of the $Co_{0.5}Pt_{0.5}$ sample was calculated with different site occupation factors p for the cobalt and platinum atoms. Occupation factors of the structural positions with the two atoms in the CoPt intermetallic (for 1a structural positions, Co $p = x$, Pt $p = 1 - x$ and for 1d—Pt $p = x$, Co $p = 1 - x$, where p may vary from 0.5 for a random solid solution to 1 for an intermetallic) were refined using the full-profile method. When the patterns matched, the obtained value of p was entered in the formula $a = 2(p - 0.5) \cdot 100\%$.

The crystallite sizes of nanoparticles were obtained using the Scherrer equation.

3. Results

The synthesized metal particles consisted of aggregates that almost completely filled the caverns in the diamond substrates (Figure 1a). An investigation of the contact between the substrate diamond and the aggregate revealed that the aggregates in most cases repeated the micro-relief shape of the individual cavern (Figure 1c).

Although the synthesized metal particles were observed only in the form of a layer coating the initial flat surface of these diamond crystals, which flaked off almost immediately following the first manipulation with the crystals, metal aggregates inside caverns were preserved on the etched surface throughout this study. A detailed investigation of the morphology of the synthesized metal aggregates showed that these aggregates comprise numerous particles whose individual size does not exceed 70 nm (Figure 1b). In the experiment, the boundaries between individual particles were clearly visible at 500 °C (Figure 1b), while, at 800 °C, such boundaries were almost absent. As a result of sintering

metal particles, the entire aggregate appeared as a continuous solid mass with rare individual particles discernable on its surface (Figure 1d). Moreover, the size and the appearance of the nanoparticles did not depend upon the size of the cavern in which they were located.

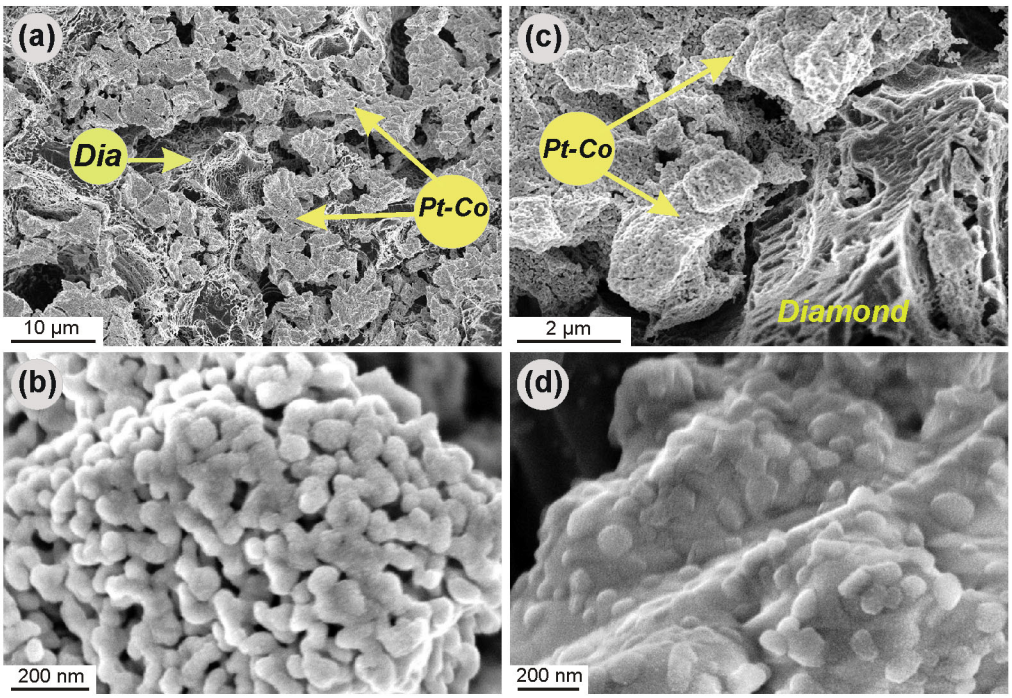

Figure 1. Aggregates of Pt–Co nanoparticles on the porous surface of an etched diamond substrate: (**a**) general view of caverns filled with metal aggregates (arrows Pt–Co) and enlarged view of nanoparticles inside the caverns (**c**); the etched diamond is marked as Dia on (**a**) and Diamond on (**c**). The synthesized nanoparticles following experiments at 500 °C (**b**) and at 800 °C (**d**), respectively, are depicted. Note that nanoparticles on (**d**) are fused into a solid mass, while on (**b**), the boundaries between individual nanoparticles can be clearly observed.

An energy-dispersive X-ray study (EDX) of the composition of the synthesized particles showed an equiatomic ratio of the metals (Figure 2).

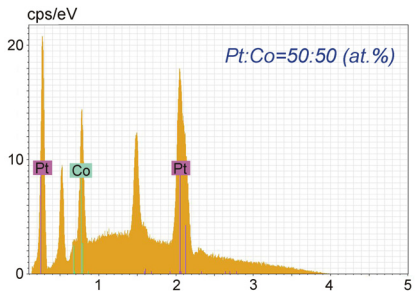

Figure 2. EDX data for CoPt sample deposited on diamond; metal ratio of Pt:Co is 1:1.

The results of X-ray phase analysis performed using a PDF database [38] are presented in Figure 3. The simulation of the diffraction patterns for Pt–Co nanoparticles located inside the caverns indicates the single-phase nature of the nanoparticles obtained.

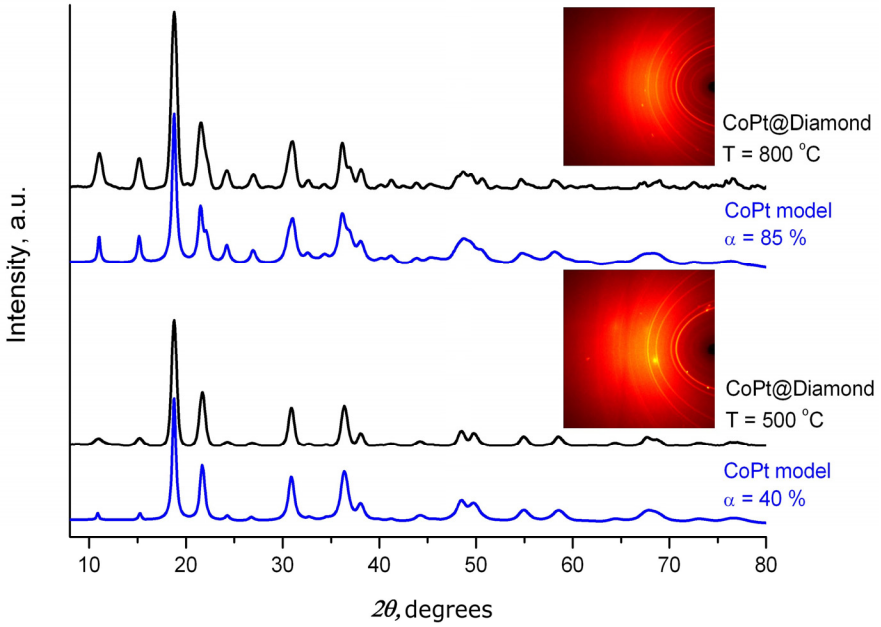

Figure 3. XRD patterns (diffractometer Bruker DUO, λ = 0.7093165 Å, D = 35 mm, 2θD = 42°) for bimetallic nanoalloys Pt–Co obtained via thermolysis of $[Co(H_2O)_6][Pt(NO_2)_4]\cdot 2H_2O$ and annealing in the hydrogen atmosphere at various temperatures (500 and 800 °C). Black curves—experimental XRD pattern under molybdenum irradiation; blue curves—model XRD patterns of different ordering degrees (α, %). Insets show lauegrams obtained from stationary samples.

As evidenced by the appearance of superstructural reflections in the range of angles between 11.04 and 15.18 degrees 2θ, the sample produced at a temperature of 500 °C corresponds to a partially ordered solid solution. According to the technique we described earlier, the degree of superstructural ordering was 40% [41–43]. The unit cell parameters were as follows: *P*4/mmm space group—a = 2.673(2), c = 3.735(3) Å, c/a = 1.397(1); crystallite sizes—10–13 nm. The sample obtained at a temperature of 800 °C showed an 85% superstructural ordering degree, while the unit cell parameters were as follows: space group *P*4/mmm—a = 2.688(2), c = 3.697(3) Å, c/a = 1.375(1); crystallite sizes—10–13 nm. The values obtained are in good agreement with the data we obtained for a pure sample [42,43].

4. Discussion

The key objective of the present study was to characterize bimetallic particles present on the diamond substrate. To achieve this, we used a thermochemical etching method to treat natural diamonds using Fe particles. This technique has already demonstrated its high effectiveness [29,32–34]; determining the distribution of metal particles on the diamond as well as the characteristics of the etched surface mainly depended upon the method of preparation of the etchant [44]. According to this procedure, the size of the pores obtained through thermochemical treatment can be decreased significantly [31,45]; however, in the present work, we aimed to produce caverns of a relatively large size. This approach was intended to facilitate the study of particle distribution both inside small individual pores and within large caverns. In this context, it is important to note that the porous surface obtained after the etching and further removal of Fe particles in acids consisted completely of diamond material.

Although the synthesis of Pt–Co nanoparticles occurred over the entire surface of the diamonds, as our SEM study shows, the nanoparticles forming the object of investigation remained only throughout the etched area. Both individual metal particles and their small groups were found to be anchored to the surface irregularities on cavern walls produced through etching (Figure 4).

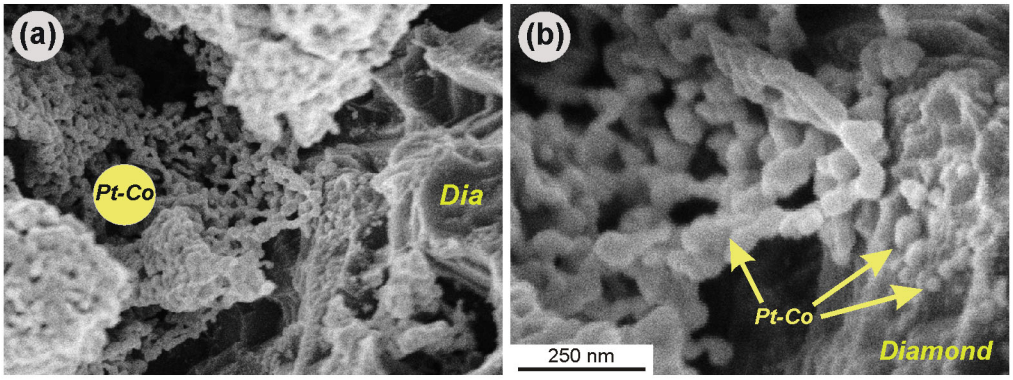

Figure 4. Contact of an aggregate of Pt–Co nanoparticles synthesized at 500 °C with a wall of a diamond substrate: (**a**) general view; (**b**) enlarged view of the same area—the nanoparticles are attached to the diamond in the areas with surface irregularities; individual nanoparticles are located within the pores throughout the diamond (marked with an arrow); Dia—diamond.

It can be assumed that the porous surface of the etched diamond acted as a host for individual metal particles or their small groups, thus fixing the main aggregate of Pt–Co nanoparticles within the cavern structure (Figure 5). This result confirms the effectiveness of thermochemical etching for treating a diamond surface prior to the deposition of metal nanoparticles. The similar appearance of nanoparticles presented both inside small and large caverns indicates that diamond acted as an inert support only, i.e., the synthesis process was not influenced by the cavern size.

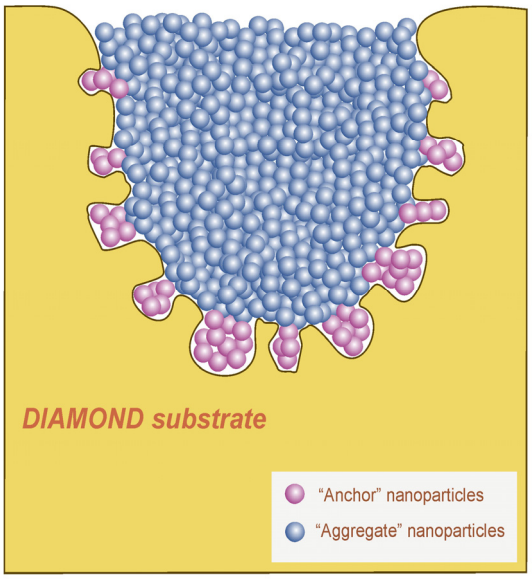

Figure 5. Schematic vertical cross section of a substrate diamond after the experiments: etch cavern on the diamond surface is filled with Pt–Co nanoparticles (as shown in Figure 1a,c). A group of nanoparticles (marked as "Anchor" nanoparticles) were located within small relief elements inside the cavern wall, thus "anchoring" the main aggregate of Pt–Co nanoparticles, which filled the whole cavern.

When studying the ordering process of $Pt_{0.50}Co_{0.50}$ solid solutions in [46], we established the kinetic dependences between the degree of ordering and crystallite sizes versus the annealing time (Figure 6).

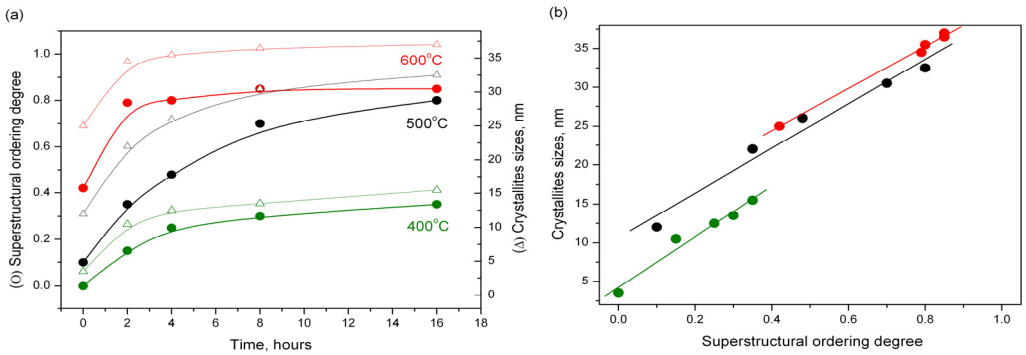

Figure 6. Kinetic dependences between the degree of ordering (marked by ●) and crystallite sizes (marked by Δ) versus annealing (**a**) and correlation between the sizes of crystallites and the superstructural ordering degree (**b**).

The correlation between the sizes of crystallites and the superstructural ordering degree is apparent. One of the goals of the present work was to determine whether it is possible to obtain a solid solution with a high degree of superstructural ordering without a significant increase in the size of crystallites due to the limitation of sample mass transfer. As the calculations from the XRD data show, this aim was achieved. While maintaining the crystallite sizes at 10–13 nm, the sample annealed at a temperature of 800 °C showed a higher degree of superstructural ordering.

The dense filling of the caverns with aggregates of synthesized nanoparticles observed in our experiments (Figure 1a) reflects the certain concentration of an initial substance applied in the solution. At the same time, the uniform filling of the porous surface in our experiment means that the metal nanoparticles were evenly distributed over the entire surface of the substrate. Of course, it is possible to fill the pores with different amounts of metal nanoparticles by varying the concentration of starting precursor compound in the solution, while given the hemispherical shape of the etching channels and their sufficiently large depth, a large portion of the synthesized nanomaterial can be deposited inside the pores, and the lower concentration of the starting precursor will produce a synthesized material that is mainly present in the form of individual nanoparticles located within small relief elements on the cavern walls. In the latter case, the nanoscale alloys will be separated in space and no mass transfer between neighboring particles will occur. Such reactors can be useful for studying the superstructural ordering in particles limited by the cavern volume, which likely strongly affects the magnetic properties of such objects. In summary, synthesized bimetallic Pt–Co particles were shown to be embedded in the diamond surface. First of all, the diamond served as a substrate; here, the properties of synthesized nanoparticles were similar to those obtained for other kinds of substrates. It is important to note that similar works have demonstrated the electrochemical and electrocatalytic characterization of metal particles once deposited on a boron-doped diamond (BDD) substrate [22]. The BDD was chosen due to its remarkable properties of chemical inertness, low background current, and good mechanical resistance to chemical and electrochemical attacks. Due to these properties, the BDD electrode was used for the study of supported particles to avoid certain problems encountered with other common substrates (corrosion, oxide formation, etc.). They are good electrocatalysts of ethanol oxidation.

The results of the present work, consisting mainly of the cavernous surface of a diamond crystal with metallic material embedded within small surface sculptures, have implications for discussions on some aspects of the genesis of diamonds in nature. A currently popular hypothesis describes the formation of diamonds of hundreds or even thousands of carats in size during subduction processes occurring with the participation of metals [47–49]. The morphology of such diamond crystals is typically very complex, as indicated by detailed studies of the multiple changes occurring in their internal structure between the stages of growth and dissolution [50]. In experiments carried out in Fe-based systems, it was shown that various surface sculptures can form on diamond crystals

through dissolution [51,52]. Such etching sculptures not only mimic the textures observed on natural diamond crystals, but also indicate that many natural diamonds came into contact with Fe-based metals in the Earth's mantle. If such metals are involved in the production of even a part of these morphological series, the role of Fe-based metals in the genesis of natural diamonds becomes significant. When dissolution conditions change to the growth stage, such sculptures will be overgrown by new diamond matter. In this case, a possibility of capturing the metallic material within the cavernous surface of a diamond inevitably arises, thereby forming metallic inclusions. At later stages, metallic inclusions are able to migrate through diamonds [53], leading to crystal self-purification [54]. While on the one hand, this may explain the high purity of large natural diamonds, it also indicates a certain role of carbon matter in the overall percolation of metal melts in the Earth's mantle [55].

Metals can either form a "pocket" where diamonds grow/dissolve or migrate further to be deposited within silicate rocks of the mantle. The following mechanism of the process can be assumed. When reaching a temperature conforming at a definite pressure to the appearance of a melt at the iron–carbon interface, the percolation of iron into the graphite/diamond-filled interstices between silicate minerals commences along with the dissolution of carbon in the melt. As a result, metal fills the interstitial volume occupied by graphite/diamond. The proposed mechanism of molten iron percolation, implying diamond and graphite in a silicate matrix under high pressure, can help to overcome the problem of high dihedral angles between metallic melt and silicates to explain the early differentiation of the Earth and other planetary bodies. As noted above, the migration of iron within diamond crystals is possible under the gradient of temperatures via the dissolution–recrystallization mechanism. Additionally, even in a solid state, in the presence of hydrogen, Fe particles can move along the grain boundaries of diamond crystals according to a process of carbon hydrogenolysis [29,32,33], in which iron plays the role of a catalyst but does not form reaction products.

One more important practical aspect of the present work should be noted. Since metals of compositions as synthesized in our experiments are not found as inclusions either in natural diamonds [56] or in lab-grown systems [57], the presence of such particles as Pt–Co bimetallic alloys within a diamond either implies their artificial origin or that they should be considered as an exotic natural case. As shown in this study, such particles can be identified using analytical methods according to their morphology, composition, structure, or ratio of components. Therefore, the results obtained in this experimental work demonstrate the possibility of using bimetallic Pt–Co alloy nanoparticles as markers for diamond crystals for the purpose of their subtle identification. Such an approach could find application in identifying gem-quality diamonds, as well as expensive diamond tools or high-tech elements made of large diamond crystals.

5. Conclusions

The results of the present work demonstrate that a thermochemically etched diamond crystal can serve as a substrate for the deposition of bimetallic particles on its surface. The synthesized nanoalloys were single-phase $Pt_{0.50}Co_{0.50}$ solid solutions with different degrees of structural ordering: 40% at a synthesis temperature of 500 °C, and 85% at 800 °C. Both nanoalloys had a tetragonal space group, *P*4/mmm, and crystallite sizes of 10–13 nm. The ratio of a unit cell parameter *c/a* decreased with increasing superstructural ordering from 1.397(1) for 40% to 1.375(1) for the 800 °C sample. The possibility of obtaining a solid solution with a high degree of superstructural ordering without a significant increase in the size of crystallites due to the limitation of sample mass transfer has been demonstrated.

We propose that the thermochemically treated surface of diamond crystals can serve as a reactor for studying the magnetic properties of particles embedded in surface caverns. With a decrease in cavern size, the synthesized objects can serve as objects of study in further research on the phase transformations of bi- and polymetallic particles of a given size without mass transfer between neighboring particles. Although natural diamond

crystals were used as a process model, the obtained results are generally applicable to different diamond types, including natural, synthetic HPHT, or CVD diamonds, as well as boron-doped diamonds (BDDs). This work has demonstrated the anchoring effect of metallic materials within small surface sculptures of natural diamond, which implies significant capturing of metals during the changing stages of dissolution and growth in the deep Earth. Additionally, the demonstrated etching of natural diamond crystals, followed by the synthesis of the Pt–Co bimetallic particles embedded within the surface caverns, represents an opportunity to carry out subtle markings on diamond crystals. The potential objects of such subtle markings can be both gem-quality diamonds and high-tech elements made of large diamonds.

Author Contributions: E.F. and A.C. conceived and designed the experiment. A.Z. carried out the deposition of metals on diamonds. V.S., S.G. and E.Z. performed the experimental measurements. E.F. and A.C. carried out the data analysis and wrote the paper. All authors have read and agreed to the published version of the manuscript.

Funding: This research was funded by the Russian Science Foundation, grant number 23-27-00129 (Egor Zhimulev).

Data Availability Statement: The original contributions presented in the study are included in the article; further inquiries can be directed to the corresponding author.

Conflicts of Interest: The authors declare no conflict of interest.

References

1. Ferrando, R.; Jellinek, J.; Johnston, R.L. Nanoalloys: From theory to applications of alloy clusters and nanoparticles. *Chem. Rev.* **2008**, *108*, 845–910. [CrossRef] [PubMed]
2. Cai, R.; Ellis, P.R.; Yin, J.; Liu, J.; Brown, C.M.; Griffin, R.; Chang, G.; Yang, D.; Ren, J.; Cooke, K.; et al. Performance of Preformed Au/Cu Nanoclusters Deposited on MgO Powders in the Catalytic Reduction of 4-Nitrophenol in Solution. *Small* **2018**, *14*, 1703734. [CrossRef] [PubMed]
3. Zaytsev, S.Y.; Plyusnin, P.E.; Slavinskaya, E.M.; Shubin, Y.V. Synthesis of bimetallic nanocompositions Au_xPd_{1-x}/γ-Al_2O_3 for catalytic CO oxidation. *J. Nanopart. Res.* **2019**, *19*, 367. [CrossRef]
4. Piccolo, L.; Li, Z.Y.; Demiroglu, I.; Moyon, F.; Konuspayeva, Z.; Berhault, G.; Afanasiev, P.; Lefebvre, W.; Yuan, J.; Johnston, R.L. Understanding and controlling the structure and segregation behaviour of AuRh nanocatalysts. *Sci. Rep.* **2016**, *6*, 35226. [CrossRef] [PubMed]
5. Savk, A.; Özdil, B.; Demirkan, B.; Nas, M.S.; Calimli, M.H.; Alma, M.H.; Inamuddin Asiri, A.M.; Şen, F. Multiwalled carbon nanotube-based nanosensor for ultrasensitive detection of uric acid, dopamine, and ascorbic acid. *Mater. Sci. Eng. C* **2019**, *99*, 248–254. [CrossRef] [PubMed]
6. Zhu, X.; Guo, Q.; Sun, Y.; Chen, S.; Wang, J.-Q.; Wu, M.; Fu, W.; Tang, Y.; Duan, X.; Chen, D.; et al. Optimising surface d charge of AuPd nanoalloy catalysts for enhanced catalytic activity. *Nat. Commun.* **2019**, *10*, 1428. [CrossRef]
7. Filatov, E.Y.; Semushina, Y.P.; Gosteva, A.N. Obtaining and catalytic properties investigation of the products of double complex salts $[Cr(ur)_6][M(L)_6]$ thermal oxidation (M=Co, Fe; L=CN^-, $1/2C_2O_4^{2-}$). *J. Therm. Anal. Calorim.* **2018**, *134*, 355–361. [CrossRef]
8. Zadesenets, A.V.; Garkul, I.A.; Filatov, E.Y.; Plyusnin, P.E.; Filippov, T.N.; Asanova, T.I.; Korolkov, I.V.; Baidina, I.A.; Asanov, I.P.; Korenev, S.V. Oxalato complexes of Pd(II) with Co(II) and Ni(II) as single-source precursors for bimetallic nanoalloys. *J. Therm. Anal. Calorim.* **2019**, *138*, 111–121. [CrossRef]
9. Potemkin, D.I.; Filatov, E.Y.; Zadesenets, A.V.; Snytnikov, P.V.; Shubin, Y.V.; Sobyanin, V.A. Preferential CO oxidation over bimetallic Pt–Co catalysts prepared via double complex salt decomposition. *Chem. Eng. J.* **2012**, *207–208*, 683–689. [CrossRef]
10. Potemkin, D.I.; Filatov, E.Y.; Zadesenets, A.V.; Sobyanin, V.A. CO preferential oxidation on $Pt_{0.5}Co_{0.5}$ and Pt-CoOx model catalysts: Catalytic performance and operando XRD studies. *Catal. Commun.* **2017**, *100*, 232–236. [CrossRef]
11. Potemkin, D.I.; Filatov, E.Y.; Zadesenets, A.V.; Rogozhnikov, V.N.; Gerasimov, E.Y.; Snytnikov, P.V.; Korenev, S.V.; Sobyanin, V.A. Bimetallic Pt-Co/η-Al_2O_3/FeCrAl wire mesh composite catalyst prepared via double complex salt $[Pt(NH_3)_4][Co(C_2O_4)_2(H_2O)_2]\cdot 2H_2O$ decomposition. *Mater. Lett.* **2019**, *236*, 109–111. [CrossRef]
12. Potemkin, D.I.; Konishcheva, M.V.; Zadesenets, A.V.; Snytnikov, P.V.; Filatov, E.Y.; Korenev, S.V.; Sobyanin, V.A. Bimetallic $Pt_{0.5}Co_{0.5}/SiO_2$ Catalyst: Preparation, Structure, and Properties in Preferential Oxidation of Carbon Monoxide. *Kinet. Catal.* **2019**, *59*, 514–520. [CrossRef]
13. Churakova, E.M.; Badmaev, S.D.; Snytnikov, P.V.; Gubanov, A.I.; Filatov, E.Y.; Plyusnin, P.E.; Belyaev, V.D.; Korenev, S.V.; Sobyanin, V.A. Bimetallic Rh–Co/ZrO_2 Catalysts for Ethanol Steam Conversion into Hydrogen-Containing Gas. *Kinet. Catal.* **2010**, *51*, 893–897. [CrossRef]

14. Artini, C.; Muolo, M.L.; Passerone, A. Diamond-metal interfaces in cutting tools: A review. *J. Mater. Sci.* **2012**, *47*, 3252–3264. [CrossRef]
15. Field, E.J. (Ed.) *The Properties of Natural and Synthetic Diamond*; Academic Press: London, UK, 1992; p. 710. [CrossRef]
16. Hyde, M.E.; Jacobs, R.; Compton, R.G. In Situ AFM Studies of Metal Deposition. *J. Phys. Chem. B* **2002**, *106*, 11075–11080. [CrossRef]
17. Fujishima, A.; Einaga, Y.; Rao, T.N.; Tryk, D.A. *Diamond Electrochemistry*; Elsevier Amsterdam-BKC: Tokyo, Japan, 2005; p. 586.
18. Salazar-Banda, G.R.; Suffredini, H.B.; Avaca, L.A. Improved Stability of PtOx Sol-Gel-Modified Diamond Electrodes Covered with a Nafion® Film. *J. Bras. Chem. Soc.* **2005**, *16*, 903–906. [CrossRef]
19. Welch, C.M.; Hyde, M.E.; Banks, C.E.; Compton, R.G. The Detection of Nitrate Using In-Situ Copper Nanoparticle Deposition at a Boron Doped Diamond Electrode. *Anal. Sci.* **2005**, *21*, 1421–1430. [CrossRef]
20. Simm, A.O.; Ji, X.; Banks, C.E.; Hyde, M.E.; Compton, R.G. AFM studies of metal deposition: Instantaneous nucleation and the growth of cobalt nanoparticles on boron-doped diamond electrodes. *ChemPhysChem* **2006**, *7*, 704–709. [CrossRef]
21. Siné, G.; Duo, I.; El Roustom, B.; Fóti, G.; Comninellis, C. Deposition of clusters and nanoparticles onto boron-doped diamond electrodes for electrocatalysis. *J. Appl. Electrochem.* **2006**, *36*, 847–862. [CrossRef]
22. Siné, G.; Fóti, G.; Comninellis, C. Boron-doped diamond (BDD)-supported Pt/Sn nanoparticles synthesized in microemulsion systems as electrocatalysts of ethanol oxidation. *J. Electroanal. Chem.* **2006**, *595*, 115–124. [CrossRef]
23. La-Torre-Riveros, L.; Abel-Tatis, E.; Méndez-Torres, A.E.; Tryk, D.A.; Prelas, M.; Cabrera, C.R. Synthesis of platinum and platinum–ruthenium-modified diamond nanoparticles. *J. Nanopart. Res.* **2011**, *13*, 2997–3009. [CrossRef]
24. Masuda, H.; Watanabe, M.; Yasui, K.; Tryk, D.A.; Rao, T.N.; Fujishima, A. Fabrication of a nanostructured diamond honeycomb film. *Adv. Mater.* **2000**, *12*, 444–447. [CrossRef]
25. Honda, K.; Rao, T.N.; Tryk, D.A.; Fujishima, A.; Watanabe, M.; Yasui, K.; Masuda, H. Fabrication of through-hole diamond membranes by plasma etching using anodic porous alumina mask. *Electrochem. Solid State* **2001**, *4*, 101–103. [CrossRef]
26. Li, C.Y.; Hatta, A. Electronic and structural properties on nanowhiskers fabricated on iron coated diamond films by radio frequency O_2 plasma etching. *J. New Mater. Electrochem. Syst.* **2007**, *10*, 221–224.
27. Kuroshima, H.; Makino, T.; Yamasaki, S.; Matsumoto, T.; Inokuma, T.; Tokuda, N. Mechanism of anisotropic etching on diamond (111) surfaces by a hydrogen plasma treatment. *Appl. Surf. Sci.* **2017**, *422*, 452–455. [CrossRef]
28. Ralchenko, V.G.; Kononenko, T.V.; Pimenov, S.M.; Chernenko, N.V.; Loubnin, E.N.; Armeyev, V.Y.; Zlobin, A.Y. Catalytic interaction of Fe, Ni and Pt with diamond films: Patterning applications. *Diam. Relat. Mater.* **1993**, *2*, 904–909. [CrossRef]
29. Sonin, V.M.; Chepurov, A.I.; Fedorov, I.I. The action of iron particles at catalyzed hydrogenation of {100} and {110} faces of synthetic diamond. *Diam. Relat. Mater.* **2003**, *12*, 1559–1562. [CrossRef]
30. Ohashi, T.; Sugimoto, W.; Takasu, Y. Catalytic etching of {100}-oriented diamond coating with Fe, Co, Ni, and Pt nanoparticles under hydrogen. *Diam. Relat. Mater.* **2011**, *20*, 1165–1170. [CrossRef]
31. Chepurov, A.; Sonin, V.; Shcheglov, D.; Latyshev, A.; Filatov, E.; Yelisseyev, A. A highly porous surface of synthetic monocrystalline diamond: Effect of etching by Fe nanoparticles in hydrogen atmosphere. *Int. J. Refract. Met. Hard Mater.* **2018**, *76*, 12–15. [CrossRef]
32. Chepurov, A.I.; Sonin, V.M.; Dereppe, J.-M. The channeling action of iron particles in the catalyzed hydrogenation of synthetic diamond. *Diam. Relat. Mater.* **2000**, *9*, 1435–1438. [CrossRef]
33. Chepurov, A.I.; Sonin, V.M.; Shamaev, P.P. Using catalytic hydrogenolysis for brazing diamond tools. *Weld. Int.* **2002**, *16*, 978–980. [CrossRef]
34. Chepurov, A.I.; Sonin, V.M.; Shamaev, P.P.; Yelisseyev, A.P.; Fedorov, I.I. The action of iron particles at catalyzed hydrogenation of natural diamond. *Diam. Relat. Mater.* **2002**, *11*, 1592–1596. [CrossRef]
35. Chepurov, A.; Sonin, V.; Shcheglov, D.; Zhimulev, E.; Sitnikov, S.; Yelisseyev, A.; Chepurov, A. Surface Porosity of Natural Diamond Crystals after the Catalytic Hydrogenation. *Crystals* **2021**, *11*, 1341. [CrossRef]
36. Zadesenets, A.V.; Filatov, E.Y.; Plyusnin, P.E.; Asanova, T.I.; Baidina, I.A.; Slyakhova, E.V.; Asanov, I.P.; Korenev, S.V. Complex salts of Pd(II) and Pt(II) with Co(II) and Ni(II) aqua-cations as single-source precursors for bimetallic nanoalloys and mixed oxides. *New J. Chem.* **2018**, *42*, 8843–8850. [CrossRef]
37. Prescher, C.; Prakapenka, V.B. DIOPTAS: A program for reduction of two-dimensional X-ray diffraction data and data exploration. *High Press. Res.* **2015**, *35*, 223–230. [CrossRef]
38. International Centre for Diffraction Data. *Powder Diffraction File, PDF-2/Release 2010*; International Centre for Diffraction Data: Newtown Square, PA, USA, 2010.
39. Fashinformationszentrum Karlsruhe. *Inorganic Crystal Structure Database/ICSD, Release 2018*; Fashinformationszentrum Karlsruhe: Eggenstein-Leopoldshafen, Germany, 2018.
40. Kraus, W.; Nolze, G. *PowderCell 2.4*; Federal Institute for Materials Research and Testing: Berlin, Germany, 2000.
41. Zadesenets, A.; Filatov, E.; Plyusnin, P.; Baidina, I.; Dalezky, V.; Shubin, Y.; Korenev, S.; Bogomyakov, A. Bimetallic single-source precursors $[M(NH_3)_4][Co(C_2O_4)_2(H_2O)_2]\cdot 2H_2O$ (M = Pd, Pt) for the one run synthesis of CoPd and CoPt magnetic nanoalloys. *Polyhedron* **2011**, *30*, 1305–1312. [CrossRef]
42. Komogortsev, S.V.; Chizhik, N.A.; Filatov, E.Y.; Korenev, S.V.; Shubin, Y.V.; Velikanov, D.A.; Iskhakov, R.S.; Yurkin, G.Y. Magnetic properties and $L1_0$ phase formation in CoPt nanoparticles. *Solid State Phenom.* **2012**, *190*, 159–162. [CrossRef]

43. Komogortsev, S.V.; Iskhakov, R.S.; Zimin, A.A.; Filatov, E.Y.; Korenev, S.V.; Shubin, Y.V.; Chizhik, N.A.; Yurkin, G.Y.; Eremin, E.V. The exchange interaction effects on magnetic properties of the nanostructured CoPt particles. *J. Magn. Magn. Mater.* **2016**, *401*, 236–241. [CrossRef]
44. Chepurov, A.I.; Sonin, V.M.; Chepurov, A.A.; Zhimulev, E.I.; Tolochko, B.P.; Yelisseyev, V.S. Interaction of diamond with ultrafine Fe powders prepared by different procedures. *Inorg. Mater.* **2011**, *47*, 864–868. [CrossRef]
45. Sonin, V.M. Interaction of fine Fe particles with structural defects on {111} faces of synthetic diamond crystals in a hydrogen atmosphere. *Inorg. Mater.* **2004**, *40*, 20–22. [CrossRef]
46. Komogortsev, S.V.; Iskhakov, R.S.; Zimin, A.A.; Filatov, E.Y.; Korenev, S.V.; Shubin, Y.V.; Chizhik, N.A.; Yurkin, G.Y.; Eremin, E.V. Magnetic anisotropy and order parameter in nanostructured CoPt particles. *Appl. Phys. Lett.* **2013**, *103*, 152104. [CrossRef]
47. Smith, E.M.; Shirey, S.B.; Nestola, F.; Bullock, E.S.; Wang, J.; Richardson, S.H.; Wang, W. Large gem diamonds from metallic liquid in Earth's deep mantle. *Science* **2016**, *354*, 1403–1405. [CrossRef] [PubMed]
48. Nestola, F. Inclusions in super-deep diamonds: Windows on the very deep Earth. *Rend. Lincei Sci. Fis. E Nat.* **2017**, *28*, 595–604. [CrossRef]
49. Daver, L.; Bureau, H.; Boulard, E.; Gaillou, E.; Cartigny, P.; Pinti, D.L.; Belhadj, O.; Guignot, N.; Foy, E.; Estève, I.; et al. From the lithosphere to the lower mantle: An aqueous-rich metal-bearing growth environment to form type IIb blue diamonds. *Chem. Geol.* **2022**, *613*, 121163. [CrossRef]
50. Afanasiev, V.; Ugapeva, S.; Babich, Y.; Sonin, V.; Logvinova, A.; Yelisseyev, A.; Goryainov, S.; Agashev, A.; Ivanova, O. Growth story of one diamonds: A window to the lithospheric mantle. *Minerals* **2022**, *12*, 1048. [CrossRef]
51. Sonin, V.M.; Zhimulev, E.I.; Pomazanskiy, B.S.; Zemnuhov, A.L.; Chepurov, A.A.; Afanasiev, V.P.; Chepurov, A.I. Morphological features of diamond crystals dissolved in $Fe_{0.7}S_{0.3}$ melt at 4 GPa and 1400 degrees C. *Geol. Ore Depos.* **2018**, *60*, 82–92. [CrossRef]
52. Chepurov, A.I.; Sonin, V.M.; Zhimulev, E.I.; Chepurov, A.A.; Pomazansky, B.S.; Zemnukhov, A.L. Dissolution of diamond crystals in a heterogeneous (metal-sulfide-silicate) medium at 4 GPa and 1400 °C. *J. Mineral. Petrol. Sci.* **2018**, *113*, 59–67. [CrossRef]
53. Chepurov, A.A.; Dereppe, J.M.; Fedorov, I.I.; Chepurov, A.I. The change of Fe-Ni alloy inclusions in synthetic diamond crystals due to annealing. *Diam. Relat. Mater.* **2000**, *9*, 1374–1379. [CrossRef]
54. Fedorov, I.I.; Chepurov, A.I.; Chepurov, A.A.; Kuroedov, A.V. Estimation of the rate of postcrystallization self-purification of diamond from metal inclusions in the earth's mantle. *Geochem. Int.* **2005**, *43*, 1235–1239.
55. Zhimulev, E.I.; Chepurov, A.I.; Sonin, V.M.; Litasov, K.D.; Chepurov, A.A. Experimental modeling of percolation of molten iron through polycrystalline olivine matrix at 2.0–5.5 GPa and 1600 °C. *High Press. Res.* **2018**, *38*, 153–164. [CrossRef]
56. Stachel, T.; Harris, J.W. The origin of cratonic diamonds—Constraints from mineral inclusions. *Ore Geol. Rev.* **2008**, *34*, 5–32. [CrossRef]
57. Fedorov, I.I.; Chepurov, A.I.; Sonin, V.M.; Chepurov, A.A.; Logvinova, A.M. Experimental and thermodynamic study of the crystallization of diamond and silicates in a metal-silicate-carbon system. *Geochem. Int.* **2008**, *46*, 340–350. [CrossRef]